Archives of Hydro-Engineering and Environmental Mechanics
Vol. 57 (2010), No. 1, pp. 61–79

Simulation of Dam-Break Flow by a Corrected Smoothed Particle Hydrodynamics Method

Ryszard Staroszczyk

Institute of Hydro-Engineering, Polish Academy of Sciences,
ul. Kościerska 7, 80-328 Gdańsk, Poland, e-mail: rstar@ibwpan.gda.pl

(Received December 18, 2009; revised April 08, 2010)

Abstract

The paper deals with numerical modelling of water flow which is generated by the break of a dam. The problem is solved by applying a smoothed particle hydrodynamics (SPH) method in which standard smoothing kernel functions are corrected in such a way that so-called linear reproducing conditions for kernel approximations and their gradients are satisfied. The proposed SPH model has been used to simulate a two-dimensional problem of the collapse of a water column inside a rectangular tank. The simulations illustrate the formation and subsequent propagation of a wave over the horizontal plane. It is shown that the model predictions of the changes of the advancing wave-front position, and of the changes of the free surface elevation of water, compare well with experimental data. Also, the results obtained with the corrected SPH method are compared with those given by the standard SPH method with no kernel correction. In addition, an impact of the surging wave against a vertical rigid wall is illustrated.

Key words: Dam-break problem, free-surface flow, meshfree Lagrangian method, smoothed particle hydrodynamics

Notations

a	–	reference particle label,
b	–	neighbouring particle label,
d	–	characteristic particle spacing,
h	–	kernel smoothing length,
H	–	initial water column height,
L	–	initial water column width,
m	–	mass,
N	–	number of particles in a support domain,
p	–	pressure,
r	–	distance between particles,
R	–	kernel support domain radius,
t	–	time,

$\boldsymbol{v}$ – velocity vector,
V – volume,
W – smoothing kernel function,
x_i $(i = 1, 2, 3)$ – spatial Cartesian coordinates,
$\boldsymbol{x}$ – position vector,
ϱ – density.

1. Introduction

Since its invention, independently, by Lucy (1977) and Gingold and Monaghan (1977), the Smoothed Particle Hydrodynamics (SPH) method has been extended considerably, to become one of the most versatile and computationally effective discrete particle methods used in the fields of physics, applied mechanics and engineering. The growing significance of the method can be attributed to its several attractive features, such as conceptual simplicity, relative ease of programming, and its natural capability of dealing with problems involving large deformations. Being a fully meshfree Lagrangian approach, the SPH method has found successful applications in numerical modelling of a wide range of phenomena, such as dynamic impact (Johnson et al 1996), damage and fracture of metals (Randles and Libersky 1996), sea (Gutfraind and Savage 1997) and river (Shen et al 2000) floating ice dynamics, flows through porous media (Morris et al 1999), heat transfer processes (Cleary and Monaghan 1999), underwater explosions (Liu et al 2003*b*).

Naturally, the SPH method has also been used to solve various hydrodynamics problems, including those which are of importance to hydro- and off-shore engineering. For example, Monaghan (1996) employed this method to investigate gravity currents and solitary waves in water; Lo and Shao (2002) analysed the run-up and run-down of solitary waves at a vertical wall and on a sloping beach; Colagrossi and Landrini (2003) studied the classical dam-break problem, including the analysis of water impact against a wall; Gómez-Gesteira et al (2005) investigated the phenomenon of a wave overtopping a flat rigid horizontal plate; Dalrymple and Rogers (2006) modelled two- and three-dimensional problems of a wave breaking on a sloping beach; Antoci et al (2007) studied a fluid–elastic structure interaction problem; and most recently Ataie-Ashtiani et al (2008) investigated the problem of the run-up of a tsunami wave on a sloping beach.

In the above papers devoted to hydrodynamics problems, different variants of the SPH method have been applied. In earlier works, represented, for instance, by the paper of Monaghan (1996), the conventional SPH approach is followed in which water is treated as a weakly compressible fluid, and in which all field variables are approximated at discrete particles by using a single interpolating function (known in SPH as the smoothing kernel), the same for all particles, irrespective of their positions and the positions of neighbouring particles, within the fluid domain. In later works, various improvements have been gradually introduced, with the aim

of achieving better modelling of the real fluid behaviour on one hand, and to increase the accuracy of computations on the other. Hence, attempts have been made to model water as an incompressible fluid, which is a common simplification in problems involving the phenomena of gravity wave propagation. Representative examples of such formulations (sometimes referred to as Incompressible SPH, or I-SPH) are the papers by Lo and Shao (2002) and Ataie-Ashtiani et al (2008). A typical feature of these formulations is the necessity to solve a Poisson equation for pressure at each time step in order to enforce the incompressibility constraint. This effectively excludes the application of fast explicit time-stepping schemes which are used in the standard SPH method, considerably increasing the computational cost of the method.

Efforts aimed at increasing the accuracy and stability of the SPH formulations have addressed a variety of numerical issues, though it seems that the most promising approach is that in which the smoothing kernel is constructed in such a way that it forms a *partition of unity* (Belytschko et al 1998). Since in the standard SPH approach the latter property is not satisfied exactly for a system of arbitrarily scattered discrete particles, a special *correction function* is derived, by which the original SPH kernel is multiplied so as to achieve a partition of unity. The principles on which the derivation of such corrected kernels is based are the *consistency* and *completeness* of interpolating functions, and are known from the general theory of meshfree particle methods (Belytschko et al 1998). In principle, the kernel correction of an approximation function, or its spatial derivatives, or both, is possible – a general methodology for constructing such corrected kernels has been developed by Liu et al (2003*a*).

In the context of free-surface water flows, the above corrected SPH approach has been followed, among others, by Colagrossi and Landrini (2003) and Dalrymple and Rogers (2006). The former authors employed one of the methods proposed by Belytschko et al (1998), while the latter applied a kernel correction method known as Shepard filtering. In both cases, only the correction of approximation functions is performed. In this paper, in addition to the approximation functions, correction of their gradients (first-order spatial derivatives) is also carried out. This modification improves the accuracy of the SPH kernel approximation, albeit at an increased computational expense. The proposed method is applied to solving a classical two-dimensional dam-break problem, with the flow occurring in the vertical plane, in order to examine the numerical performance of the model compared to a simpler, and computationally more economic, standard SPH formulation in which no kernel correction is performed.

The paper is organized as follows. In Section 2 fundamental equations expressing the conservation and constitutive laws that have been adopted in this study are presented. Then, in Section 3, a brief summary of the SPH methodology is given, followed by discrete formulations of equations describing the problem considered. The section is concluded with a description of the time-stepping method used

to integrate the SPH equations. In the following Section, 4, results of numerical simulations are presented, and, finally, some conclusions are given in Section 5.

2. Problem Formulation

In this work, water is treated as a compressible inviscid liquid, and it is assumed that its motion, occurring in isothermal conditions, is entirely due to the action of gravity. The fluid mass conservation balance is defined, in local form, by the continuity equation

$$\frac{\mathrm{D}\varrho}{\mathrm{D}t} + \varrho \nabla \cdot \boldsymbol{v} = 0, \tag{1}$$

where $\mathrm{D}/\mathrm{D}t$ denotes the material (convected) time derivative, ϱ is the fluid density, t is time, $\boldsymbol{v}$ is the fluid velocity vector, and ∇ is the nabla operator. The linear momentum balance, expressing the Euler equation of motion, is given by

$$\varrho \frac{\mathrm{D}\boldsymbol{v}}{\mathrm{D}t} = -\nabla p + \varrho \boldsymbol{b}, \tag{2}$$

where p is pressure, and $\boldsymbol{b}$ denotes the body force vector. In the problem considered here, the only body force is that due to gravity.

The fluid flow is assumed to be barotropic, in which case the pressure is uniquely determined by the fluid density. The following constitutive law connecting the pressure p and density ϱ is usually adopted in the SPH method (Batchelor 1967, Monaghan 1992):

$$p(\varrho) = P_0 \left[\left(\frac{\varrho}{\varrho_0} \right)^{\gamma} - 1 \right]. \tag{3}$$

In the above equation, P_0 and ϱ_0 denote the reference pressure and density, and the parameter γ is usually taken as 7 for water and 1.4 for air (Colagrossi and Landrini 2003). The corresponding speed of sound, c_s, is given by

$$c_s = \sqrt{\frac{\gamma P_0}{\varrho_0}}. \tag{4}$$

In practical implementations, the parameters P_0, ϱ_0 and γ are selected in such a way that the maximum local fluctuations of density ϱ around the reference value ϱ_0 are of order 1% or less. The advantage of the equation of state (3), providing a direct relationship between pressure and density, is that there is no necessity to solve any additional equation for pressure (which is the Poisson equation in the case of an incompressible fluid flow). Therefore, fast explicit time-stepping algorithms can be employed in computations, avoiding the use of implicit schemes required when the Poisson equation has also to be solved as part of the solution.

3. SPH Methodology and Equations

In the SPH method, any system under consideration is represented by a collection of arbitrarily scattered discrete particles, each of which carries, in a Lagrangian sense, individual information on all physical properties relevant to the problem concerned, such as mass, density, momentum, temperature, etc. Since no connectivity for the particles is needed, the method has a fully meshfree character. Field variables are approximated by employing special interpolating functions, the smoothing kernels in the SPH terminology. These functions represent weightings with which material particles contribute to the value of a field function at a given spatial/material point. Usually, the kernel function is constructed in such way that it has non-zero values only within a finite domain, called the support domain, which means that for any field point only a limited number of neighbouring particles are involved in the interpolation. This important feature of the SPH approach, for a plane problem, is illustrated in Fig. 1, in which W denotes a smoothing kernel, and R is the radius of its circular support domain.

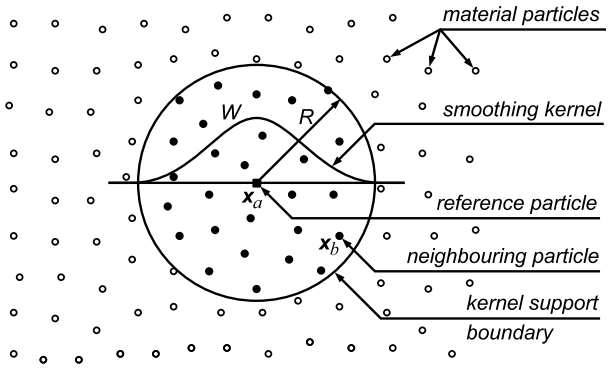

Fig. 1. The method of approximation of field variables in the SPH. The approximation at a reference particle $\boldsymbol{x}_a$ (solid square) involves material particles $\boldsymbol{x}_b$ (solid circles) situated within a circular support domain of radius R centred at $\boldsymbol{x}_a$. Particles outside the support domain (empty circles) do not contribute to the approximation of field functions at the reference particle $\boldsymbol{x}_a$

Let $\boldsymbol{x}$ be the position vector, and a and b be labels of a pair of material particles. Then, the value of any field variable $f(\boldsymbol{x})$ at particle a (so-called reference particle), located at position $\boldsymbol{x}_a$, is evaluated by means of the kernel function W centred at this particle. Owing to the compactness of the kernel support domain, only the particles situated inside this domain (those indicated by solid circles in the figure) are involved in the interpolation. This is expressed by the formula

$$f(\boldsymbol{x}_a) = \sum_{b=1}^{N} V_b \, f_b \, W(r,h)\,, \tag{5}$$

where $f_b = f(\boldsymbol{x}_b)$ is the discrete value of f at particle b, V_b is the volume of particle b, and N is the number of particles within the kernel support.

The smoothing kernel W is a function of two arguments. r is the distance between particles a and b, that is,

$$r = |\boldsymbol{x}_a - \boldsymbol{x}_b|, \tag{6}$$

and h is the so-called kernel smoothing length which determines the size of the support domain, and hence the resolution of the discretization (the number of particles involved in kernel interpolations).

There are a variety of possible kernel functions (Monaghan 1992, Liu and Liu 2003), with the Gaussian and the cubic and quintic spline functions being probably the most widely used in implementations. In this work, a modified Gaussian kernel, proposed by Colagrossi and Landrini (2003), is applied, which, in contrast to the common Gaussian distribution function, has a compact support. Hence, in two dimensions, the following form is adopted:

$$W(r,h) = \frac{C}{h^2} \begin{cases} \left[\exp\left(-q^2\right) - \exp\left(-Q^2\right)\right], & q < Q, \\ 0, & q \geq Q, \end{cases} \tag{7}$$

where

$$q = \frac{r}{h} \quad \text{and} \quad Q = \frac{R}{h}, \tag{8}$$

and the normalizing factor C is given by

$$C = \frac{1}{2\pi} \int_0^Q \left[\exp\left(-q^2\right) - \exp\left(-Q^2\right)\right] \mathrm{d}q. \tag{9}$$

3.1. Standard SPH Equations

In order to derive discrete forms of equations describing a given problem, one needs discrete approximations of differential operators. There are several methods available in SPH to construct the approximations of the gradient and divergence operators. Here, we use the forms preferred by Monaghan (1992). Accordingly, the gradient of a scalar function f at particle a is interpolated by

$$(\nabla f)_a = \varrho_a \sum_{b=1}^{N} m_b \left(\frac{f_a}{\varrho_a^2} + \frac{f_b}{\varrho_b^2}\right) \nabla_a W_{ab}\,, \tag{10}$$

and, similarly, the divergence of a vector field $\boldsymbol{f}$ at particle a is interpolated by

$$(\nabla \cdot \boldsymbol{f})_a = -\frac{1}{\varrho_a} \sum_{b=1}^{N} m_b\, \boldsymbol{f}_{ab} \cdot \nabla_a W_{ab}\,, \tag{11}$$

with m_b denoting the mass of particle b. The following notations are used:

$$W_{ab} = W(|\boldsymbol{x}_{ab}|, h), \quad \boldsymbol{f}_{ab} = \boldsymbol{f}_a - \boldsymbol{f}_b\,,$$

and $\nabla_a W_{ab}$, defined by

$$\nabla_a W_{ab} = \frac{\boldsymbol{x}_{ab}}{|\boldsymbol{x}_{ab}|} \frac{\partial W(|\boldsymbol{x}_{ab}|, h)}{\partial |\boldsymbol{x}_{ab}|}\,, \tag{12}$$

denotes the gradient of the kernel function W, taken with respect to the coordinates of particle a. Since the adopted kernel (7) is symmetric, that is $W_{ab} = W_{ba}$, then the identity holds:

$$\nabla_a W_{ab} = -\nabla_b W_{ba}\,. \tag{13}$$

The approximations (10) and (11), when used in the equations of continuity (1) and motion (2), yield the following discrete forms of the equations:

$$\frac{\mathrm{d}\varrho_a}{\mathrm{d}t} = \sum_{b=1}^{N} m_b\, \boldsymbol{v}_{ab} \cdot \nabla_a W_{ab} \tag{14}$$

and

$$\frac{\mathrm{d}\boldsymbol{v}_a}{\mathrm{d}t} = -\sum_{b=1}^{N} m_b \left(\frac{p_a}{\varrho_a^2} + \frac{p_b}{\varrho_b^2} \right) \nabla_a W_{ab} + \boldsymbol{b}_a\,. \tag{15}$$

The latter two forms are known to conserve exactly (Monaghan 1992, Li and Liu 2004) the mass and linear momentum of a system of material particles.

3.2. Corrected SPH Equations

As already stated in the Introduction, the standard SPH kernel does not form a partition of unity, since, in general, $\sum_{b=1}^{N} W_{ab} V_b \neq 1$ for a set of irregularly distributed discrete particles. For particles located in the interior of the fluid domain (at distances larger than R – the kernel support radius – from the fluid boundaries) the discrepancy from unity is usually of order which is comparable with that in other discrete methods. However, for particles situated on or near the boundaries, the interpolation error is significantly larger in view of the fact that part of the particle support domain is not filled with neighbouring particles. This can seriously affect the performance of the SPH method, leading to the appearance of numerical oscillations of pressures on/or near the boundaries, which can result in rapid deterioration of the numerical solution.

In order to reduce the spurious oscillations near the fluid boundaries, a number of methods aiming at restoring the partition of unity of the SPH kernel functions has been developed (Randles and Libersky 1996, Dilts 1999, Bonet and Kulasegaram 2000). It seems that from among these methods, the group of formulations proposed by Belytschko et al (1998), derived within the framework of the general theory of

interpolation functions for meshless discrete methods, belong to the most consistent and computationally efficient. One of these methods is adopted here – the one which corrects both the SPH kernel functions and their gradients. Accordingly, for the two-dimensional case, the corrected kernel, $\widetilde{W}_{ab}$, and the two corrected components of the kernel gradient along the x and z coordinate axes, $(\nabla_a \widetilde{W}_{ab})_x$ and $(\nabla_a \widetilde{W}_{ab})_z$, are expressed in terms of the standard kernel functions as follows:

$$\begin{aligned} \widetilde{W}_{ab} &= (c_{11} + c_{12}\, x_{ab} + c_{13}\, z_{ab})\, W^S_{ab}, \\ \left(\nabla_a \widetilde{W}_{ab}\right)_x &= (c_{21} + c_{22}\, x_{ab} + c_{23}\, z_{ab})\, W^S_{ab}, \\ \left(\nabla_a \widetilde{W}_{ab}\right)_z &= (c_{31} + c_{32}\, x_{ab} + c_{33}\, z_{ab})\, W^S_{ab}, \end{aligned} \tag{16}$$

where W^S_{ab} denotes the so-called Shepard function defined by

$$W^S_{ab} = \frac{W_{ab}}{\sum\limits_{b=1}^{N} V_b\, W_{ab}}. \tag{17}$$

Note that the Shepard functions represent a partition of unity, since $\sum_{b=1}^{N} W^S_{ab} V_b = 1$ at any particle a in the domain, irrespective whether it is near, or far from, the boundary.

The coefficients $c_{\alpha\beta}(\boldsymbol{x})$ $(\alpha, \beta = 1, 2, 3)$ in (16) are determined by applying the completeness conditions for interpolating functions and their derivatives, formulated by Belytschko et al (1998). These conditions yield the matrix equation

$$\boldsymbol{A}\boldsymbol{c}^T = \boldsymbol{I}, \tag{18}$$

in which $\boldsymbol{c}$ is the matrix of unknown coefficients $c_{\alpha\beta}$, $\boldsymbol{I}$ is the unit matrix, and $\boldsymbol{A}$ is given by

$$\boldsymbol{A} = \sum_{b=1}^{N} V_b\, W^S_{ab} \begin{pmatrix} 1 & x_{ab} & z_{ab} \\ x_{ab} & x^2_{ab} & x_{ab}\, z_{ab} \\ z_{ab} & z_{ab}\, x_{ab} & z^2_{ab} \end{pmatrix}. \tag{19}$$

The above correction procedure requires, in two dimensions, the generation and subsequent inversion of the 3×3 matrix $\boldsymbol{A}$ for each discrete particle a. The resulting corrected kernel functions and their gradients, calculated from (16) once (18) is solved for $c_{\alpha\beta}$, are used to replace respective standard SPH counterparts in the equations of continuity and motion, given by (14) and (15).

3.3. Time Integration of the SPH Equations

The problem to be solved numerically can be summarized by the following set of first-order differential equations

$$\frac{\mathrm{d}\varrho_a}{\mathrm{d}t} = M_a\,, \quad \frac{\mathrm{d}\boldsymbol{v}_a}{\mathrm{d}t} = \boldsymbol{F}_a\,, \quad \frac{\mathrm{d}\boldsymbol{x}_a}{\mathrm{d}t} = \boldsymbol{U}_a\,, \tag{20}$$

which have to be integrated for all material particles in the discrete system. The interaction terms M_a and $\boldsymbol{F}_a$ follow from the mass and momentum conservation balances. By adopting their discrete forms defined by (14) and (15), with the corrected forms of kernels and their gradients, though, one has

$$M_a = \sum_{b=1}^{N} m_b\, \boldsymbol{v}_{ab} \cdot \nabla_a \widetilde{W}_{ab}\,, \tag{21}$$

$$\boldsymbol{F}_a = -\sum_{b=1}^{N} m_b \left(\frac{p_a}{\varrho_a^2} + \frac{p_b}{\varrho_b^2} \right) \nabla_a \widetilde{W}_{ab} + \boldsymbol{b}_a\,. \tag{22}$$

The term $\boldsymbol{U}_a$ in the third equation in (20) represents a corrected velocity of particle a. The velocity correction is performed by employing the formula proposed by Monaghan (1992):

$$\boldsymbol{U}_a = \boldsymbol{v}_a + \varepsilon \sum_{b=1}^{N} \frac{m_a}{\bar{\varrho}_{ab}}\, \boldsymbol{v}_{ba} \widetilde{W}_{ab}\,, \quad \bar{\varrho}_{ab} = \frac{\varrho_a + \varrho_b}{2}\,, \tag{23}$$

in which the velocity of a given particle a is smoothed out by means of an average velocity of all neighbours b located within the kernel support of a. In this way, particle inter-penetration is prevented, thus assuring a more orderly and regular pattern of particles compared to the standard SPH approach. According to Monaghan, $0 < \varepsilon < 1$ in (23); in the subsequent numerical simulations the value $\varepsilon = 0.5$ was taken. For consistency, the corrected velocities $\boldsymbol{U}_a$, instead of $\boldsymbol{v}_a$, should also be used in the density evolution equation, that is, in the term M_a defined by (21).

In this work, the system of evolution equations (20) is solved by applying an explicit time-stepping scheme of a predictor-corrector type, in which, within each time step, the calculations proceed in two stages. Let a current time increment be defined by instants t^k and t^{k+1}, so that the time step length is $\Delta t = t^{k+1} - t^k$. Then, in the first stage, the particle density, velocity and position are calculated at the mid-step time $t^{k+1/2} = \frac{1}{2}(t^k + t^{k+1})$ by the formulae

$$\begin{aligned} \varrho_a^{k+\frac{1}{2}} &= \varrho_a^k + \frac{\Delta t}{2} M_a^k\,, \\ \boldsymbol{v}_a^{k+\frac{1}{2}} &= \boldsymbol{v}_a^k + \frac{\Delta t}{2} \boldsymbol{F}_a^k\,, \end{aligned} \tag{24}$$

$$\boldsymbol{x}_a^{k+\frac{1}{2}} = \boldsymbol{x}_a^k + \frac{\Delta t}{2}\,\boldsymbol{U}_a^k .$$

Next, using the above half-step values of density, the pressures $p_a^{k+1/2}$ are calculated from the constitutive law (3). These pressures, together with the predictions (24), yield, in turn, the half-step values of the interaction terms $M_a^{k+1/2}$ and $\boldsymbol{F}_a^{k+1/2}$, given by (21) and (22), and the half-step velocities $\boldsymbol{U}_a^{k+1/2}$, defined by (23).

In the second stage of the current time step calculations, the latter mid-step values of interaction terms are employed to evaluate the respective values at the end of the time step, at $t = t^{k+1}$, according to the equations

$$\begin{aligned} \varrho_a^{k+1} &= \varrho_a^k + \Delta t\, M_a^{k+\frac{1}{2}} , \\ \boldsymbol{v}_a^{k+1} &= \boldsymbol{v}_a^k + \Delta t\, \boldsymbol{F}_a^{k+\frac{1}{2}} , \\ \boldsymbol{x}_a^{k+1} &= \boldsymbol{x}_a^k + \Delta t\, \boldsymbol{U}_a^{k+\frac{1}{2}} . \end{aligned} \tag{25}$$

Finally, the pressures p_a^{k+1} are updated by using the above end-step values of densities in the constitutive law (3), before the terms M_a^{k+1}, $\boldsymbol{F}_a^{k+1}$ and $\boldsymbol{U}_a^{k+1}$ are determined from (21), (22) and (23) to start the next time integration step.

It is known from SPH literature (Colagrossi and Landrini 2003, Dalrymple and Rogers 2006) that it is difficult to achieve, in particular near the fluid free surfaces, a full consistency between particle mass, density and volume when one uses the density evolution equation following from the continuity equation (1). Therefore, in numerical computations, the density field is periodically regularized by applying the formula

$$\varrho_a = \sum_{b=1}^{N} m_b\, \widetilde{W}_{ab} , \tag{26}$$

which is obtained from equation (5) by setting $f = \varrho$ and replacing the standard kernel W_{ab} by its corrected form $\widetilde{W}_{ab}$ (recall that $V_b\, \varrho_b = m_b$). In the simulations, the results of which are presented in the next section, the above density regularization was carried out every tenth discrete time step.

4. Numerical Simulations

The SPH model described in the preceding section has been applied to simulate the classical problem of water flow induced by a dam break. For simplicity, it is assumed that the flow is two-dimensional and occurs in the vertical plane, and the surface on which the water flows is horizontal and frictionless. The problem geometry and adopted coordinate axes are sketched in Fig. 2. Such a simple idealized geometry, featuring a rectangular column of water, of initial height H, starting to collapse under gravity due to a sudden removal of the vertical wall at $x = L$, is commonly

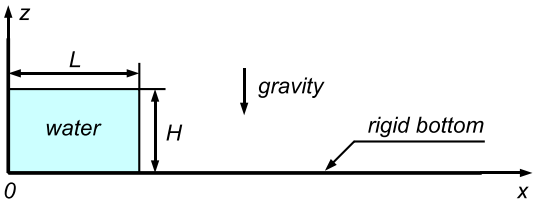

Fig. 2. Dam-break problem definition: geometric parameters and coordinate axes

used as a test case for numerical methods designed for solving rapidly varying free-surface flows.

The simulations have been performed for two aspect ratios, $L/H = 0.5$ and $L/H = 1$, since these two configurations have often been used in experimental measurements. Here, the results obtained by Martin and Moyce (1952) will be used for comparisons with the SPH model predictions, since these results seem to be the most frequently cited in the literature on dam-break problems (e.g. Zwart et al 1999, Colagrossi and Landrini 2003, Szydłowski and Zima 2006).

The results presented below have been obtained for a water column of initial height $H = 0.6$ m and initial width equal to either $L = 0.3$ m or $L = 0.6$ m. The initial water domain has been discretized by adopting a uniform grid of particles, with the same spacings in both x and z directions. Two grid resolutions have been applied: a fine one, in which the inter-particle spacing is $d = 0.01$ m; and a coarse one, in which $d = 0.02$ m. Hence, in the fine resolution grid, the total number of particles was 1800 for the $L/H = 0.5$ case, and 3600 for the $L/H = 1$ case. The respective numbers of particles in the coarse grid were 450 for $L/H = 0.5$ and 900 for $L/H = 1$. In all test cases, the SPH kernel support domain radius was taken as $R = 4d$, which means that, in the initial configuration, a typical particle inside the fluid domain had about 50 interacting neighbours. The smoothing length h, used in the kernel function W (see (7) and (8)) was equal to $4d/3$. The physical parameters appearing in the equation of state (3) were $P_0 = 10^5$ Pa and $\varrho_0 = 10^3$ kg/m^3. The evolution equations (20) were integrated with a time step of length $\Delta t = 2 \times 10^{-4}$ s. The initial conditions at $t = 0$ were those of the hydrostatic equilibrium, that is, $v_x = v_z = 0$ and $p = \varrho_0 g(H - z)$.

At the solid boundaries (vertical wall at $x = 0$ and the horizontal bottom at $z = 0$), free-slip conditions have been adopted. From among a few possible techniques of implementing such conditions and as known from the SPH literature, a method proposed by Cummins and Rudman (1999), with a slight modification, has been used. In this method, a set of so-called ghost (or virtual, or dummy) particles is added outside the walls, as illustrated in Fig. 3. These ghost particles, distributed within a strip of width R along each wall, are created, at a given time t (a given discrete time step) in such a way that they mirror the physical properties (mass, density, volume) of their physical counterparts located on the other side of the

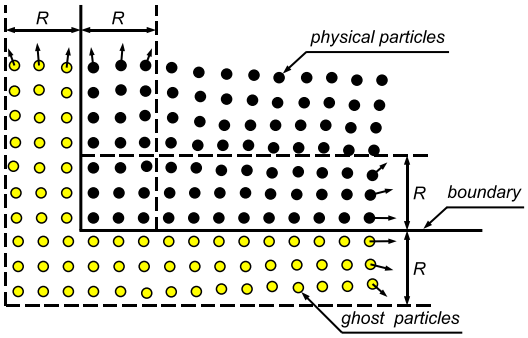

Fig. 3. Implementation of free-slip boundary conditions along solid walls. The ghost particles outside the boundaries mirror physical particles inside the fluid flow domain

wall. The x and z positions of the ghost particles are reflected with respect to the wall (hence, the two particles of each ghost/real pair are at the same distance from the wall). Further, the velocity vector components are reflected with respect to the boundary as well; that is, the tangential components of each pair of particles are the same, but the corresponding components normal to the boundary have opposite directions – in this way the condition of zero normal velocity at the boundary is enforced. In the original approach by Cummins and Rudman (1999), also the pressures at particles were mirrored across the boundary. However, it has been found here that slightly more accurate results can be obtained by assuming that the pressure at each ghost particle is increased/decreased by an amount following from the difference of the hydrostatic pressures between the positions of the ghost and its corresponding real particle.

Fig. 4 presents, for the two L/H cases considered, the results of simulations showing the evolution of the propagating water wave position. The wave front position, in a dimensionless form x/H, is expressed as a function of dimensionless time $t\sqrt{g/H}$. The numerical results are compared with experimental data measured by Martin and Moyce (1952), represented by the solid dots, and analytical results, indicated by the dashed lines, and predicted by the theory of shallow water waves (Whitham 1999). According to that theory, the wave front propagates at a constant speed of $2\sqrt{gH}$, independent of time, therefore the wave front position is a linear function of time. In the plots, the SPH results obtained by the proposed corrected method are compared with those yielded by the standard SPH approach; additionally, the results for the fine and coarse grid resolutions are compared as well (see the legend for notations). It is seen in the plots that the corrected SPH method yields, for both L/H aspect ratios, results which are in better agreement with the experiment than the standard approach with no correction of the SPH interpolating functions – this feature is more pronounced for larger values of dimensionless time. However, the increased accuracy (the better reproduction of the empirical data) requires additional computational effort: for the particular test example considered

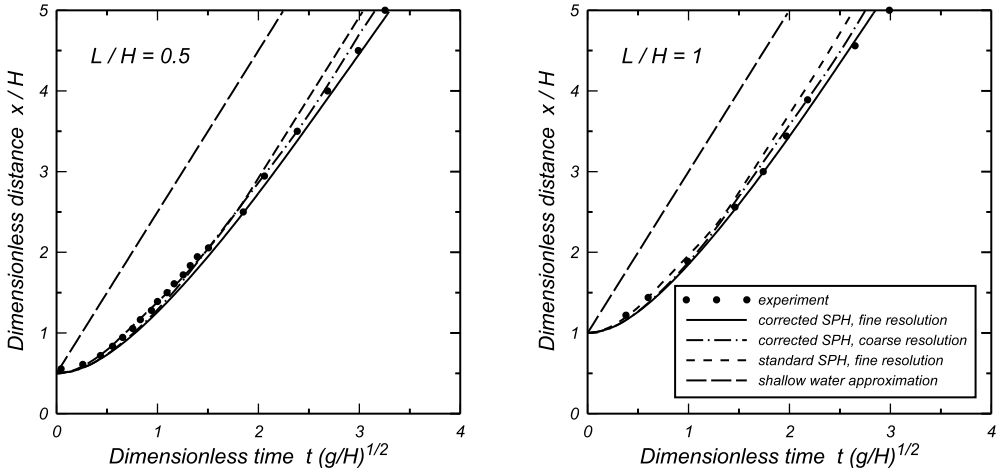

Fig. 4. Time evolution of the water front position. Comparison of numerical (lines) and experimental (solid dots) results for two aspect ratios: $L/H = 0.5$ (left plot) and $L/H = 1$ (right plot). The dashed lines show the predictions of the shallow water approximation theory

here the corrected SPH model is about 2.5 times more costly than its standard counterpart. The differences between the results given by the fine and coarse grids are relatively small, especially for shorter times. The SPH results plotted in the figure also compare favourably with results obtained by other discrete methods: a finite element solution (Zwart et al 1999), and a boundary element solution (Colagrossi and Landrini 2003).

Fig. 5 shows the evolution of the free surface elevation at $x = 0$, in which the predictions of the corrected SPH method, for both fine and coarse grid resolutions, are plotted versus the experimental results. As in Fig. 4, the results are displayed in dimensionless variables. Again, for both $L/H = 0.5$ and $L/H = 1$ cases, good agreement between the SPH results and measurements has been achieved, in particular for shorter times. Also, as in the previous figure, the differences between the results for the fine and coarse resolutions are relatively small.

The following Fig. 6 illustrates, for the case $L/H = 1$, the evolution in the water domain geometry with time elapsing from the dam-breaking instant $t = 0$. The discrete particles have been coloured according to their initial depth in the initial hydrostatic state, in order to show the changes in their mutual distribution as the flow progresses. The regular and consistent pattern of particles after a relatively long time of simulation gives confidence in the correctness of the numerical scheme used to solve the flow problem. For longer simulation times (say for $t \gtrsim 1.5$ s) the quality of the SPH solution starts to gradually deteriorate near the water front toe, as there are too few discrete particles across the water layer to ensure sufficiently accurate interpolation of the field variables.

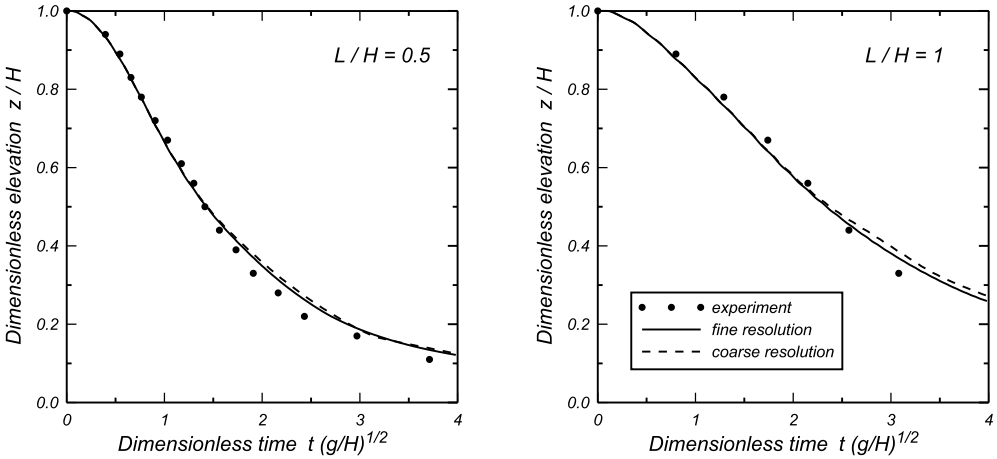

Fig. 5. Time evolution of the free surface elevation at $x = 0$. Comparison of numerical (lines) and experimental (solid dots) results for two aspect ratios: $L/H = 0.5$ (left plot) and $L/H = 1$ (right plot)

The next Fig. 7 displays the evolution of the free surface of the collapsing water column with increasing time, for $L/H = 1$. One can note the smooth variation of the free surface geometry, indicating stable behaviour of the applied numerical method. The corresponding vector plots in Fig. 8 illustrate the velocity field within the water domain for the same initial configuration as in the previous figure; shown are the fields at time levels $t = 0.3$ and $t = 0.5$ s. The velocities are given in dimensionless forms, that is, the quantities $\boldsymbol{v}/\sqrt{gH}$ are presented. Again, a smooth pattern of the plotted quantities can be observed, confirming the overall good numerical performance of the SPH method.

Finally, a dam-break flow problem involving an impact of water against a vertical rigid wall has been simulated by applying the proposed SPH model. To this aim, the configuration sketched in Fig. 9 is adopted, in which the gravity-driven flow, generated by a collapse of a water column, takes place in a rectangular tank. The simulations have been carried out for the initial water column height $H = 60$ cm, with other relevant dimensions defined in the figure. As before, it has been assumed that all solid surfaces are frictionless. In the calculations 3600 discrete particles have been used, initially distributed on a 60×60 uniform grid.

The changes of the water domain with time elapsing from the sudden removal of the vertical wall at $x = H$ are illustrated in Fig. 10. The sequence of plots shows the behaviour of water starting from the instant $t = 0.4$ s, just before the advancing water front hits the rigid wall on the right. The subsequent plots illustrate successive phases of the flow development. First the water run-up on the wall (the plot for $t = 0.8$ s), then the reversal of the flow along the wall due to the action of gravity resulting in the downward movement of the water ($t = 1.1$ s), next the plunging of the water onto the surface of the water below moving to the right ($t = 1.2$ s),

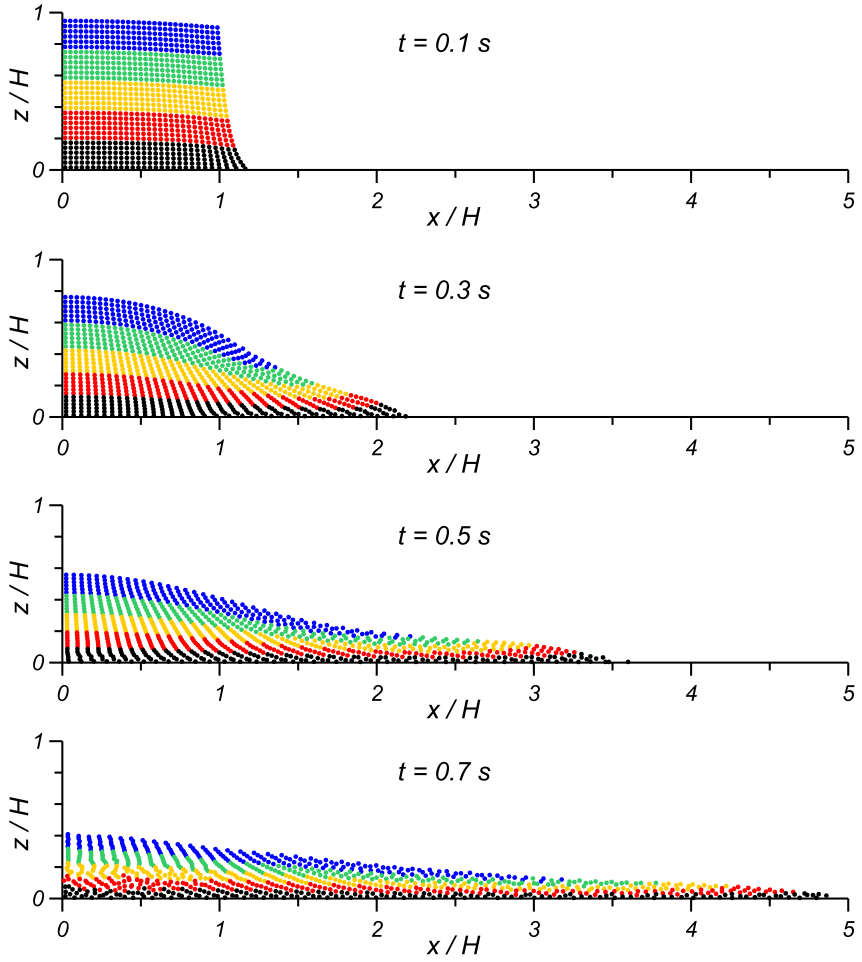

Fig. 6. Time evolution of the water domain, for the case $L/H = 1$ (900 discrete particles have been used)

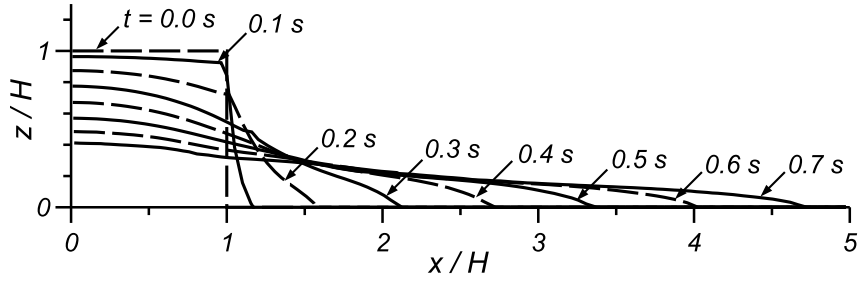

Fig. 7. Time evolution of the free surface of water, for the case $L/H = 1$ (3600 discrete particles have been used)

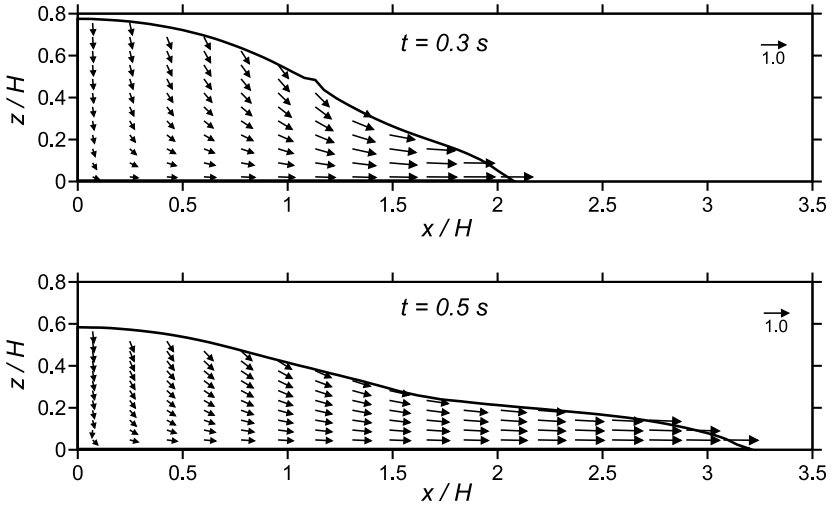

Fig. 8. Vector plots of the velocity field in water at different times, for the case $L/H = 1$ (3600 discrete particles have been used)

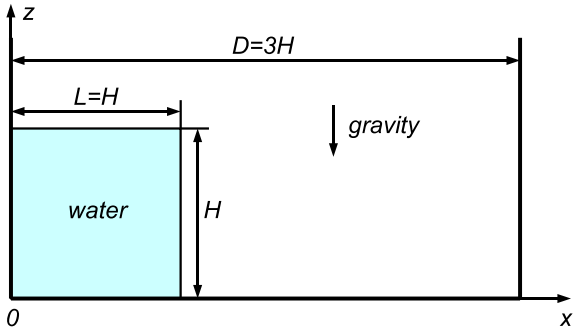

Fig. 9. Dam-break flow in a rectangular tank

followed by the water splash-up and the formation of a cavity under the jet, and the beginning of fragmentation of the flow due to some particles leaving the main body of the liquid (plots for $t = 1.3$ and 1.4 s). Note that the plots are clipped at $z = 1.6\,H$, so that the full extent of the flow along the vertical wall is not shown (the maximum run-up of the water during the simulation was about $2.38\,H$, reached at time $t \sim 1.0$ s).

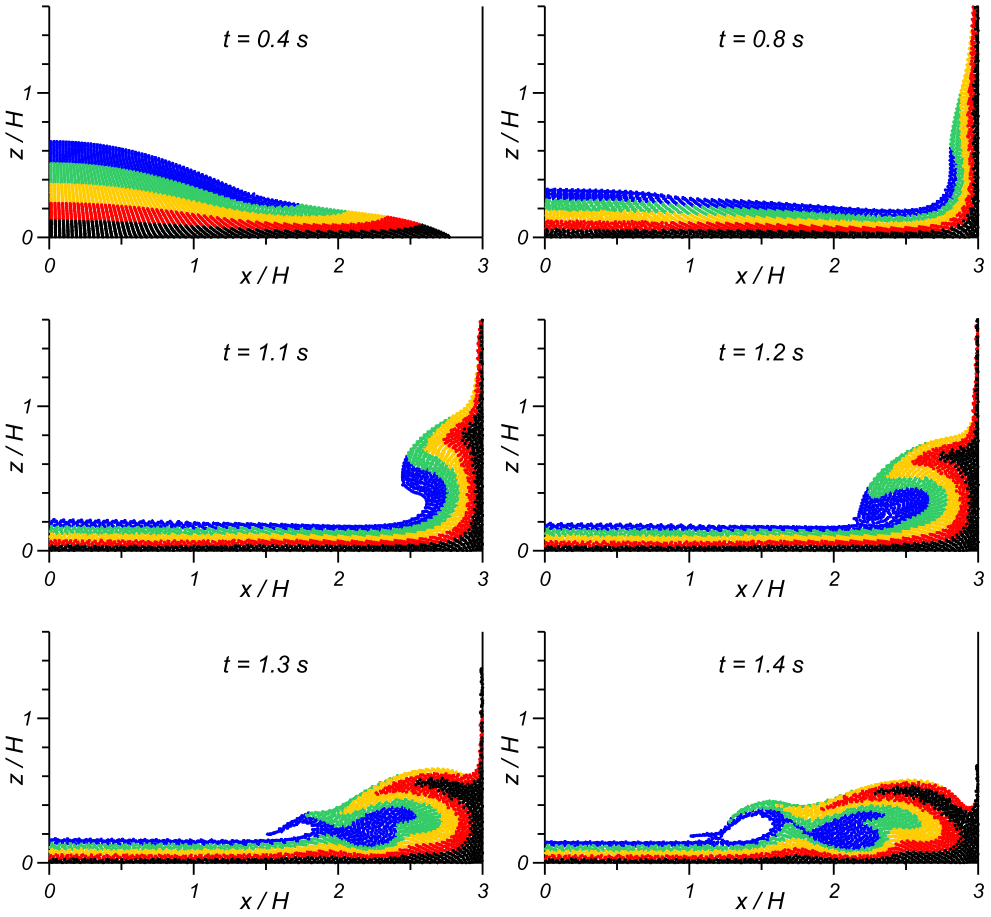

Fig. 10. Evolution of the water domain during dam-break flow in a rectangular tank (H = 60 cm, 3600 discrete particles have been used in the simulation)

5. Conclusions

In the paper, a modification of the SPH method is proposed, in which the standard kernel function and its gradient are corrected in such a way that the partition of unity property is preserved. The results of numerical simulations have shown that the kernel correction leads to better quantitative predictions of the wave front position in time than the standard SPH method, in which no correction of the kernel function is carried out. However, the improvement in accuracy is achieved at considerably increased computational cost. The results showing the time evolution of the free surface of water, and the plots of the velocity field in water, show that the method is numerically efficient and stable. Although comparable accuracy of numerical results can be achieved by employing other discrete methods, such as the finite element, finite volume or boundary element methods, it seems that the

proposed SPH approach, owing to its significantly lower computational cost and the simplicity of numerical implementation, can be considered as a serious competitor for the older and better-established methods.

References

Antoci C., Gallati M. and Sibilla S. (2007) Numerical simulation of fluid–structure interaction by SPH, *Comput. Struct.*, **85** (11–14), 879–890.

Ataie-Ashtiani B., Shobeyri G. and Farhadi L. (2008) Modified incompressible SPH method for simulating free surface problems, *Fluid Dyn. Res.*, **40** (9), 637–661.

Batchelor G. K. (1967) *An Introduction to Fluid Mechanics*, Cambridge University Press, London.

Belytschko T., Krongauz Y., Dolbow J. and Gerlach C. (1998) On the completness of meshfree particle methods, *Int. J. Numer. Meth. Eng.*, **43** (5), 785–819.

Bonet J. and Kulasegaram S. (2000) Correction and stabilization of smooth particle hydrodynamics methods with applications in metal forming simulations, *Int. J. Numer. Meth. Eng.*, **47** (6), 1189–1214.

Cleary P. W. and Monaghan J. J. (1999) Conduction modelling using smoothed particle hydrodynamics, *J. Comput. Phys.* **148** (1), 227–264.

Colagrossi A. and Landrini M. (2003) Numerical simulation of interfacial flows by smoothed particle hydrodynamics, *J. Comput. Phys.*, **191** (2), 448–475.

Cummins S. J. and Rudman M. (1999) An SPH projection method, *J. Comput. Phys.*, **152** (2), 584–607.

Dalrymple R. A. and Rogers B. D. (2006) Numerical modeling of water waves with the SPH method, *Coastal Eng.*, **53** (2–3), 141–147.

Dilts G. A. (1999) Moving-least-squares-particle hydrodynamics – I. Consistency and stability, *Int. J. Numer. Meth. Eng.*, **44** (8), 1115–1155.

Gingold R. A. and Monaghan J. J. (1977) Smoothed particle hydrodynamics: theory and application to non-spherical stars, *Mon. Not. R. Astron. Soc.*, **181**, 375–389.

Gómez-Gesteira M., Cerqueiro D., Crespo C. and Dalrymple R. A. (2005) Green water overtopping analyzed with a SPH method, *Ocean Eng.*, **32** (2), 223–238.

Gutfraind R. and Savage S. B. (1997) Marginal ice zone rheology: Comparison of results from continuum-plastic models and discrete-particle simulations, *J. Geophys. Res.*, **102** (C6), 12,647–12,661.

Johnson G. R., Stryk R. A. and Beissel S. R. (1996) SPH for high velocity impact computations, *Comput. Meth. Appl. Mech. Eng.*, **139** (1–4), 347–373.

Li S. and Liu W. K. (2004) *Meshfree Particle Methods*, Springer, Berlin.

Liu G. R. and Liu M. B. (2003) *Smoothed Particle Hydrodynamics: A Meshfree Particle Method*, World Scientific, Singapore.

Liu M. B., Liu G. R. and Lam K. Y. (2003*a*) Constructing smoothing functions in smoothed particle hydrodynamics with applications, *J. Comput. Appl. Math.*, **155** (2), 262–284.

Liu M. B., Liu G. R., Lam K. Y. and Zong Z. (2003*b*) Smoothed particle hydrodynamics for numerical simulation of underwater explosion, *Comput. Mech.*, **30** (2), 106–118.

Lo E. Y. M. and Shao S. (2002) Simulation of near-shore solitary wave mechanics by an incompressible SPH method, *Appl. Ocean Res.*, **24** (5), 275–286.

Lucy L. B. (1977) A numerical approach to the testing of the fission hypothesis, *Astron. J.*, **82** (12), 1013–1024.

Martin J. C. and Moyce W. J. (1952) An experimental study of the collapse of liquid columns on a rigid horizontal plane, *Phil. Trans. R. Soc. Lond.*, A **244**, 312–324.

Monaghan J. J. (1992) Smoothed particle hydrodynamics, *Annu. Rev. Astron. Astrophys.*, **30**, 543–574.

Monaghan J. J. (1996) Gravity currents and solitary waves, *Physica D*, **98** (2-4), 523–533.

Morris J. P., Zhu Y. and Fox J. P. (1999) Parallel simulations of pore-scale flow through porous media, *Comput. Geotech.*, **25** (4), 227–246.

Randles P. W. and Libersky L. D. (1996) Smoothed Particle Hydrodynamics: Some recent improvements and applications, *Comput. Meth. Appl. Mech. Eng.*, **139** (1–4), 375–408.

Shen H. T., Su J. and Liu L. (2000) SPH simulation of river ice dynamics, *J. Comput. Phys.*, **165** (2), 752–770.

Szydłowski M. and Zima P. (2006) Two-dimensional vertical Reynolds-averaged Navier-Stokes equations versus one-dimensional Saint-Venant model for rapidly varied open channel water flow modelling, *Arch. Hydro-Eng. Environ. Mech.*, **53** (4), 295–309.

Whitham G. B. (1999) *Linear and Nonlinear Waves*, John Wiley & Sons, New York.

Zwart P. J., Raithby G. D. and Raw M. J. (1999) The integrated space-time finite volume method and its application to moving boundary problems, *J. Comput. Phys.*, **154** (2), 497–519.